Received: 19 July 2020 | Revised: 20 August 2020 | Accepted: 1 September 2020

DOI: 10.1002/eng2.12288

SHORT COMMUNICATION

WILEY

Dual-band bandpass filter using two simple coupled microstrip rings

Jiashuai Xu[1] | **Kai-Da Xu**[2,3] | **Miao Zhang**[1] | **Qiang Chen**[3]

[1]Department of Electronic Science, Xiamen University, Xiamen, China

[2]School of Information and Communications Engineering, Xi'an Jiaotong University, Xi'an, China

[3]Department of Communications Engineering, Tohoku University, Sendai, Japan

Correspondence
Kai-Da Xu, School of Information and Communications Engineering, Xi'an Jiaotong University, Xi'an 710049, China and Department of Communications Engineering, Tohoku University, Sendai 980-8579, Japan.
Email: kaidaxu@ieee.org

Funding information
Grant-in-Aid for JSPS Research Fellow, Grant/Award Number: JP19F19350; Japan Society for the Promotion of Science, Grant/Award Number: P19350; National Natural Science Foundation of China, Grant/Award Number: 61971364

Abstract

A new dual-band bandpass filter (BPF) using two very simple coupled microstrip rings is proposed in this paper. The two identical $3\lambda_g/2$ microstrip rings are coupled each other with $\lambda_g/2$ coupled length, resulting in the generation of dual frequency bands with multiple transmission zeros (TZs). Theoretical deduction is presented to verify the proposed structure. The center frequencies and bandwidths of the two passbands can be tuned by controlling the impedance parameters of the microstrip rings. For demonstration, a prototype example of this dual-band BPF is fabricated and characterized. The measured results show that it has high selectivity and great return losses of passbands with multiple TZs at the stopband.

KEYWORDS

bandpass filters, coupled lines, dual-band, ring resonators

1 | INTRODUCTION

Multiband components such as antenna arrays[1,2] and bandpass filters (BPFs)[3,4] with high performance are in intensive demand for the applications in microwave multi-service wireless communication systems. For the designs of dual-band and tri-band BPFs, numerous methods and techniques have been proposed. The primary design strategy is to employ multiple resonators or a multi-mode resonator[5-10] for the multi-band BPF realizations. But different techniques are utilized such as stub loaded resonator methods,[5,6] substrate integrated waveguides,[7,8] high-temperature superconducting[9,10] and transversal signal interaction techniques.[11] In References 6 and 9, the researchers employed one-wavelength ring resonators with stepped impedance structures or loading stubs to obtain dual-band filtering response. In References 7 and 10, half-wavelength stub-loaded open-loop resonators or slotlines were proposed to achieve different types of dual-band BPFs. However, the designed prototypes of these filters are relatively complicated.

Due to the essential frequency selective functions, the parallel coupled lines are also widely applied in the design of filters.[12-15] In this paper, we will present a dual-band BPF using two simple coupled microstrip rings with sharp roll-off

skirts and high return losses. The generalized transmission matrix is used to characterize the BPF circuit model. The transmission and reflection coefficients of the filter are derived smoothly and the positions of the seven transmission zeros (TZs) are calculated accordingly.

2 | DESIGN AND ANALYSIS OF THE DUAL-BAND BPF

Figure 1 shows the ideal circuit of the proposed dual-band BPF, where two identical $3\lambda_g/2$ microstrip rings are coupled each other with $\lambda_g/2$ coupled length (ie, $\theta = 180°$). Note that the λ_g represents the guided wavelength corresponding to the ring resonator's eigenfrequency rather than the operating wavelength of the BPF. The even- and odd-mode characteristic impedances of the $\lambda_g/2$ parallel coupled lines are Z_{0e} and Z_{0o}, respectively. The remaining parts of the ring are the two $\lambda_g/2$ microstrip lines with characteristic impedances of Z_1 and Z_2, respectively, divided by input/output port. In order to clarify the theoretically analysis process of the dual-band BPF, the circuit nodes 1 to 10 are marked and current directions are also defined as seen in Figure 1.

The 2-port dual-band BPF can be analyzed indirectly through the derivation of 4-port circuit network (nodes 3, 4, 9, and 10), since the input/output port is split into two transmission paths. Obviously, the total transfer matrix of the 4-port network is the product of the three individual transfer matrices, expressed as

$$\begin{bmatrix} V_3 \\ I_3 \\ V_4 \\ I_4 \end{bmatrix} = M_1 \bullet M_2 \bullet M_3 \bullet \begin{bmatrix} V_9 \\ I_9 \\ V_{10} \\ I_{10} \end{bmatrix}, \tag{1}$$

where

$$M_1 = \begin{bmatrix} \cos\theta & jZ_2\sin\theta & 0 & 0 \\ j\sin\theta/Z_2 & \cos\theta & 0 & 0 \\ 0 & 0 & \cos\theta & jZ_1\sin\theta \\ 0 & 0 & j\sin\theta/Z_1 & \cos\theta \end{bmatrix}, \tag{2}$$

$$M_2 = \frac{1}{Z_{0e} - Z_{0o}} \begin{bmatrix} Z_{0e} + Z_{0o} & 2jZ_{0e}Z_{0o}\cot\theta & 0 & 2jZ_{0e}Z_{0o}/\sin\theta \\ -2j\cot\theta & -Z_{0e} - Z_{0o} & 2j/\sin\theta & 0 \\ 0 & 2jZ_{0e}Z_{0o}/\sin\theta & Z_{0e} + Z_{0o} & 2jZ_{0e}Z_{0o}\cot\theta \\ 2j/\sin\theta & 0 & -2j\cot\theta & -Z_{0e} - Z_{0o} \end{bmatrix}, \tag{3}$$

$$M_3 = \begin{bmatrix} \cos\theta & -jZ_2\sin\theta & 0 & 0 \\ -j\sin\theta/Z_2 & \cos\theta & 0 & 0 \\ 0 & 0 & \cos\theta & -jZ_1\sin\theta \\ 0 & 0 & -j\sin\theta/Z_1 & \cos\theta \end{bmatrix}. \tag{4}$$

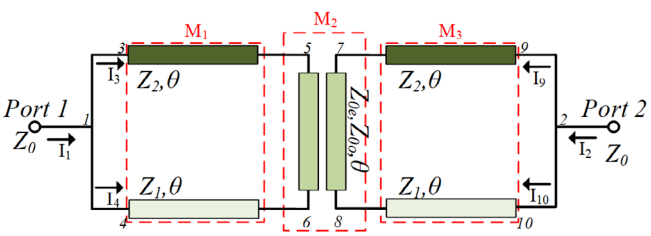

FIGURE 1 Ideal circuit of the dual-band BPF ($Z_0 = 50\,\Omega$, $\theta = 180°$)

It can be easily obtained from Kirchhoff laws that

$$V_1 = V_3 = V_4 \qquad V_2 = V_9 = V_{10}, \tag{5a}$$

$$I_1 = I_3 = I_4 \qquad I_2 = I_9 = I_{10} \tag{5b}$$

.

Note that the overall 2-port network of the proposed filter has the ABCD matrix,

$$\begin{bmatrix} V_1 \\ I_1 \end{bmatrix} = \begin{bmatrix} A & B \\ C & D \end{bmatrix} \bullet \begin{bmatrix} V_2 \\ I_2 \end{bmatrix}.$$

By substituting (2) to (6) into (1), the entries A, B, C and D can be determined analytically.

$$A = \frac{a_1 \cos\theta + a_2 \cos^2\theta + a_3(\cos^3\theta + \cos^4\theta) - 2{Z_1}^2{Z_2}^2(Z_{0e} + Z_{0e})}{a_4 Z_1 Z_2 (Z_{0\mathrm{e}} - \mathrm{Z}_{0o})}, \tag{7a}$$

$$B = \frac{2b_1(\cos\theta + 1)}{jb_2(Z_{0e} - Z_{0o})\sin\theta}, \tag{7b}$$

$$C = \frac{(2c_1 + 8{Z_1}^2{Z_2}^2 Z_{0\mathrm{e}} Z_{0o})(\cos\theta - 1)}{jb_2{Z_1}^2{Z_2}^2(Z_{0\mathrm{e}} - Z_{0o})\sin\theta}, \tag{7c}$$

$$D = A, \tag{7d}$$

where a_1, a_2, a_3, a_4, b_1, b_2 and c_1 are expressed in (8a) to (8g), as shown below.

$$a_1 = Z_1 Z_2[({Z_2}^2 - {Z_1}^2)Z_{0e} - ({Z_2}^2 + {Z_1}^2)Z_{0o} - (Z_2 + Z_1)({Z_{0e}}^2 + {Z_{0\mathrm{o}}}^2) - 2Z_1 Z_2(Z_2 + Z_1 + Z_{0e} + Z_{0\mathrm{o}})], \tag{8a}$$

$$a_2 = a_1 - 2Z_1 Z_2[(Z_{0e} Z_{0\mathrm{o}} + 1)(Z_{0e} + Z_{0\mathrm{o}}) + 2Z_{0e} Z_{0o}(Z_1 + Z_2)], \tag{8b}$$

$$\begin{aligned} a_3 = {} & 2{Z_1}^3({Z_2}^2 + Z_{0e} Z_{0\mathrm{o}}) + 2{Z_2}^3({Z_1}^2 + Z_{0e} Z_{0\mathrm{o}}) + 2Z_1 Z_2[(Z_1 + Z_2)^2(Z_{0e} + Z_{0o}) + (Z_1 + Z_2)({Z_{0e}}^2 + {Z_{0o}}^2)] \\ & + 2Z_{0e} Z_{0\mathrm{o}}[(Z_1 + Z_2)Z_{0\mathrm{o}} + ({Z_1}^2 + {Z_2}^2)(Z_{0e} + Z_{0\mathrm{o}}) + (3Z_1 + 3Z_2 + 2Z_{0e} + 2Z_{0\mathrm{o}})Z_1 Z_2], \end{aligned} \tag{8c}$$

$$a_4 = 2Z_1 Z_2(1 + \cos\theta) + ({Z_1}^2 + {Z_2}^2)(\cos^2\theta + \cos\theta) + (Z_1 + Z_2)(Z_{0e} + Z_{0o})(\cos^2\theta + \cos\theta) + 2Z_{0\mathrm{o}} Z_{0e}\cos^2\theta, \tag{8d}$$

$$b_1 = [{Z_{0e}}^2\cos^2\theta - Z_1 Z_2 + Z_1 Z_2\cos^2\theta + (Z_1 + Z_2)Z_{0e}\cos^2\theta][{Z_{0o}}^2\cos^2\theta + Z_1 Z_2\cos^2\theta + (Z_1 + Z_2)Z_{0o}\cos^2\theta - Z_1 Z_2], \tag{8e}$$

$$b_2 = [{Z_1}^2 + {Z_2}^2 + (Z_1 + Z_2)(Z_{0e} + Z_{0o}) + 2Z_{0o} Z_{0e}]\cos^2\theta + [(Z_1 + Z_2)^2 + (Z_1 + Z_2)(Z_{0e} + Z_{0o})]\cos\theta + 2Z_1 Z_2, \tag{8f}$$

$$\begin{aligned} c_1 = {} & ({Z_1}^2 Z_2 + {Z_1}^2 Z_{0o} + Z_1{Z_2}^2 + 2Z_1 Z_2 Z_{0o} + Z_1{Z_{0o}}^2 + {Z_2}^2 Z_{0o} + Z_2{Z_{0o}}^2) \\ & ({Z_1}^2 Z_2 + {Z_1}^2 Z_{0\mathrm{e}} + Z_1{Z_2}^2 + 2Z_1 Z_2 Z_{0e} + Z_1{Z_{0e}}^2 + {Z_2}^2 Z_{0e} + Z_2{Z_{0e}}^2)(\cos\theta + \cos^2\theta)^2. \end{aligned} \tag{8g}$$

Therefore, the scattering parameters of the BPF ideal circuit can be obtained according to the following equations,

$$S_{11} = \frac{AZ_0 + B - CZ_0^2 - DZ_0}{AZ_0 + B + CZ_0^2 + DZ_0}. \tag{9a}$$

$$S_{21} = \frac{2Z_0}{AZ_0 + B + CZ_0^2 + DZ_0}. \tag{9b}$$

For demonstration, Figure 2 shows the comparisons between the calculated frequency responses and *Keysight ADS* simulations of the proposed ideal BPF circuit model, which are in good agreement.

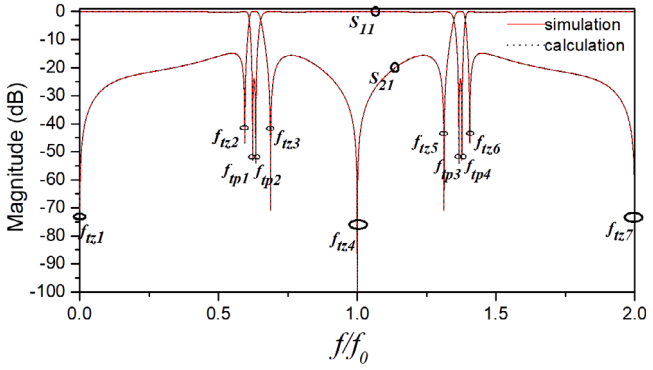

FIGURE 2 Calculated and simulated frequency responses of Figure 1 ($Z_0 = 50\,\Omega$, $Z_1 = 109.2\,\Omega$, $Z_2 = 52.4\,\Omega$, $Z_{0e} = 131.5\,\Omega$, $Z_{0o} = 90.3\,\Omega$, $\theta = 180°$)

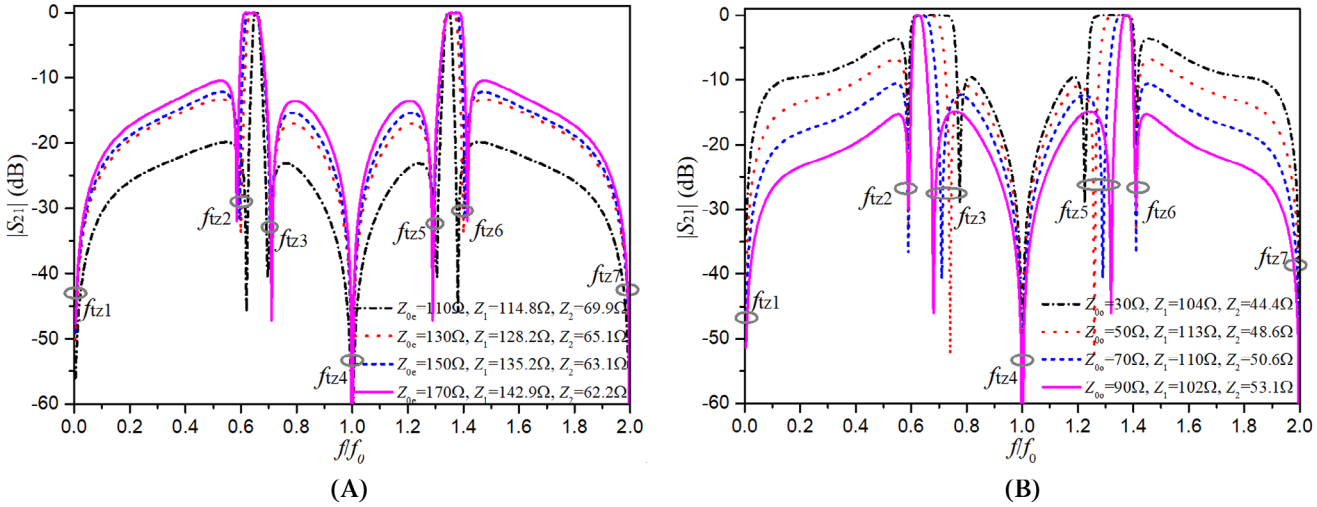

FIGURE 3 (A) Frequency response variations with different values of Z_{0e}, Z_1 and Z_2 when $Z_{0o} = 90\,\Omega$ is fixed. (B) Frequency response variations with different values of Z_{0o}, Z_1 and Z_2 when $Z_{0e} = 130\,\Omega$ is fixed

Seen from Figure 2, seven finite TZs ($f_{tz1}, f_{tz2}, f_{tz3}, f_{tz4}, f_{tz5}, f_{tz6}$ and f_{tz7}) in the stopband at the frequency range from 0 to $2f_0$ are obtained through calculation by setting $S_{21} = 0$, shown as follows,

$$f_{tz1} = 0 f_{tz4} = \pi f_{tz7} = 2\pi, \tag{10a}$$

$$f_{tz2} = \pi - \arccos\frac{E + 2Z_1Z_2 - \sqrt{F}}{E + 2Z_{0e}Z_{0o}}, \tag{10b}$$

$$f_{tz3} = \pi + \arccos\frac{E + 2Z_1Z_2 + \sqrt{F}}{E + 2Z_{0e}Z_{0o}}, \tag{10c}$$

$$f_{tz5} = 2\pi - f_{tz3}f_{tz6} = 2\pi - f_{tz2}, \tag{10d}$$

where

$$E = Z_1Z_{0e} + Z_2Z_{0e} + Z_1Z_{0o} + Z_2Z_{0o} + {Z_1}^2 + Z_2^2, \tag{11a}$$

$$\begin{aligned} F = {} & Z_1^4 + Z_2^4 - 4Z_1^3Z_2 - 4Z_1Z_2^3 + 6{Z_1}^2Z_2^2 \\ & + (2Z_1^3 - 2Z_1^2Z_2 - 2Z_1Z_2^2 + 2Z_2^3)(Z_{0e} + Z_{0o}) \\ & + (Z_1 + Z_2)^2(Z_{0e}^2 + Z_{0o}^2) + (2Z_1^2 + 2Z_2^2 - 12Z_1Z_2)Z_{0e}Z_{0o}. \end{aligned} \tag{11b}$$

The above-mentioned f_0 represents the eigenfrequency of the ring resonator rather than the center frequency of the BPF. When the characteristic impedance $Z_0 = 50\,\Omega$ and electrical length $\theta = \pi$ are fixed, four other impedance variables

Z_1, Z_2, Z_{0e} and Z_{0o} can be adjusted to control the center frequencies and bandwidths of the two passbands as shown in Figure 3. When adjusting Z_{0e}, Z_1 and Z_2 with fixed Z_{0o} in Figure 3A, the second and sixth TZs (f_{tz2} and f_{tz6}) will be shift, resulting in the movement of the left (right) edge of the first (second) passband. Similarly, when tuning Z_{0o}, Z_1 and Z_2 with fixed Z_{0e}, the third and fifth TZs (f_{tz3} and f_{tz5}) will be moved as illustrated in Figure 3B, thus the right (left) edge of the first (second) passband will be tuned accordingly. Therefore, the center frequencies and bandwidths of the two passbands can be both tuned as long as these four impedance variables are changed appropriately.

3 | IMPLEMENTATION RESULTS

To validate the proposed dual-band filter scheme, a prototype is fabricated on a F4B substrate with relative dielectric constant of 2.65 and thickness of 1 mm. The layout of this proposed filter and its fabricated photograph are shown in Figure 4. A slot etched on the metallic ground of the bottom layer is to achieve a stronger coupling effect for the coupled lines of the top layer. The simulated and measured S-parameters of the filter are given in Figure 5, which agree reasonably well with each other. The first and second passbands of the proposed dual-band BPF have the measured center frequencies at 1.33 and 2.82 GHz with 3-dB bandwidths of 100 and 80 MHz (ie, 7.5% and 2.83%), respectively. The measured insertion losses (ILs) of the two passbands are smaller than 1.16 dB and 2.46 dB, while the return losses (RLs) are better than 38 dB and 42 dB, respectively. Table 1 tabulates the performance comparisons of the proposed dual-band BPF with some previous reported works. It can be seen that the presented study has good passband RLs and ILs with multiple TZs at the stopband.

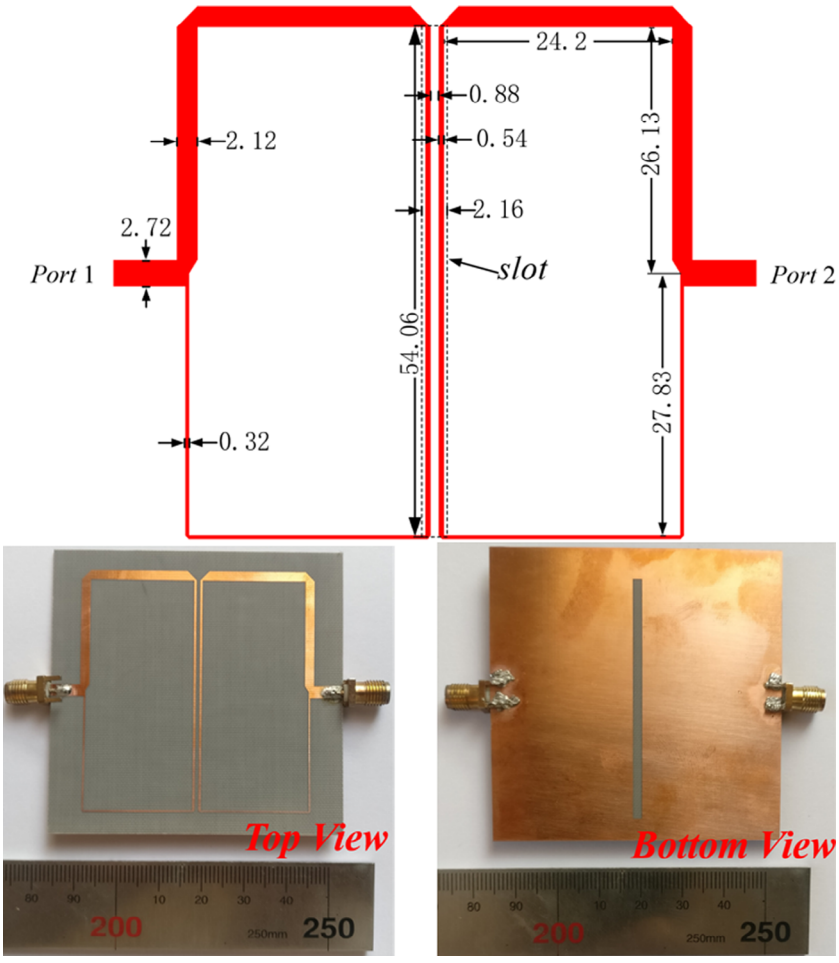

FIGURE 4 Layout of the proposed BPF (unit: mm) and its fabricated photograph

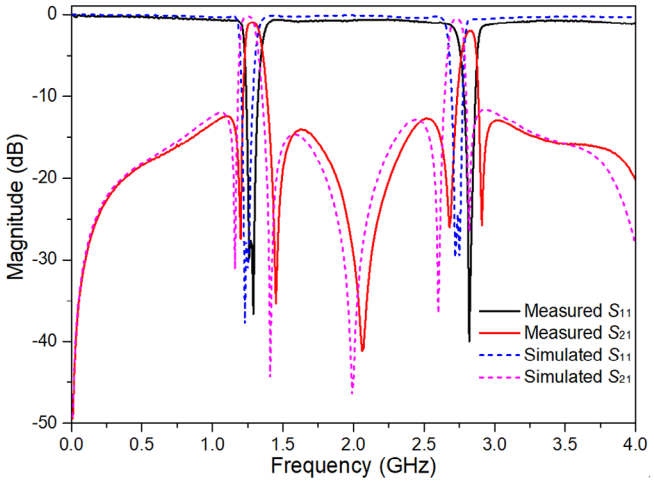

FIGURE 5 Simulated and measured S-parameters of the dual-band BPF

TABLE 1 Comparisons with some previous BPFs

	CFs (GHz)	FBWs (%)	TZs	RLs (dB)	ILs (dB)	Size (λ_g^2)
[4]B	3.6 & 7.1	8.2 & 6.7	4	14 & 14	1.3&1.2	0.29 × 0.29
[8]	3.78 & 4.82	11.3 & 10.7	6	14 & 33	1.38&1.82	1.28 × 0.05
[9]	2.4 & 5.2	8 & 3.69	4	16.4 & 16.4	1.6&2.5	NM
[10]	2.49 & 3.49	15.6 & 8.0	5	12 & 12	1.2&1.2	NM
This work	1.33 & 2.82	7.5% & 2.83%	7	38 & 42	1.16 & 2.46	0.29 × 0.30

Abbreviations: CFs, center frequencies; FBWs, 3-dB fractional bandwidths; NM, not mentioned.

4 | CONCLUSION

We have proposed a new dual-band BPF with very simple structure and good performance. Using two identical coupled microstrip rings, the filter circuit generates two passbands with multiple TZs, sharp roll-off skirts, and high return losses. The full-wave electromagnetic simulations and measurements of the demonstrative BPF are in good agreement, which validates the proposed idea.

ACKNOWLEDGEMENTS

This work was supported in part by the FY2019 JSPS Postdoctoral Fellowship for Research in Japan (Standard) under Grant P19350, in part by the Grant-in-Aid for JSPS Research Fellow under Grant JP19F19350, and in part by the National Natural Science Foundation of China under Grant 61971364.

PEER REVIEW INFORMATION

Engineering Reports thanks Xuehui Guan and other anonymous reviewers for their contribution to the peer review of this work.

PEER REVIEW

The peer review history for this article is available at https://publons.com/publon/10.1002/eng2.12288.

AUTHOR CONTRIBUTIONS

Jiashuai Xu: Formal analysis; investigation; writing-original draft. **Kai-Da Xu:** Conceptualization; funding acquisition; investigation; methodology; project administration; resources; supervision; writing-review and editing. **Miao Zhang:** Funding acquisition. **Qiang Chen:** Funding acquisition.

CONFLICT OF INTEREST

The authors declare no potential conflict of interest.

DATA AVAILABILITY STATEMENT

The data that support the findings of this study are available from the corresponding author upon reasonable request.

ORCID

Kai-Da Xu https://orcid.org/0000-0001-9408-1347

REFERENCES

1. Li W, Xu KD, Tang X, Yang Y, Liu Y, Liu QH. Substrate integrated waveguide cavity-backed slot array antenna using high-order radiation modes for dual-band applications in K-band. *IEEE Trans Antennas Propag*. 2017;65(9):4556-4565.
2. Xu K-D, Luyen H, Behdad N. A decoupling and matching network design for single- and dual-band, two-element antenna arrays. *IEEE Trans Microwave Theory Technol*. 2020;68(9):3986-3999. https://doi.org/10.1109/TMTT.2020.2989120.
3. Shi J, Lin L, Chen J-X, Chu H, Wu X. Dual-band bandpass filter with wide stopband using one stepped-impedance ring resonator with shorted stubs. *IEEE Microwave Wireless Compon Lett*. 2014;24(7):442-444.
4. Li D, Xu K-D. Compact dual-band bandpass filter using coupled lines and shorted stubs. *Electron Lett*. 2020;56(14):721-724.
5. Ai J, Zhang Y, Xu K, Li D, Fan Y. Miniaturized quint-band bandpass filter based on multi-mode resonator and λ/4 resonators with mixed electric and magnetic coupling. *IEEE Microwave Wireless Compon Lett*. 2016;26(5):343-345.
6. Xu KD, Zhang Y, Fan Y, Li JLW, Joines WT, Liu QH. Planar dual- and tri-band bandpass filters using single improved ring resonator and simple feed scheme. *Microwave Opt Technol Lett*. 2014;56(3):574-577.
7. Zhang H, Kang W, Wu W. Miniaturized dual-band SIW filters using E-shaped slotlines with controllable center frequencies. *IEEE Microwave Wireless Compon Lett*. 2018;28(4):311-313.
8. Azad AR, Mohan A. Substrate integrated waveguide dual-band and wide-stopband bandpass filters. *IEEE Microwave Wireless Compon Lett*. 2018;28(8):660-662.
9. Guan X, Le C, Ren B, et al. Compact dual-band HTS bandpass filter using coplanar waveguide short-circuited stub-loaded ring resonator. *IEEE Trans Appl Supercond*. 2019;29(5):1500704.
10. Zhou L, Li H, Long Z, Cao S, Jiang M, Zhang T. Design of high-temperature superconducting dual-band filter with multiple transmission zeros. *IEEE Trans. Appl. Supercond*. 2019;29(6):1500512.
11. Wang L-T, Xiong Y, Gong L, Zhang M, Li H, Zhao X-J. Design of dual-band bandpass filter with multiple transmission zeros using transversal signal interaction concepts. *IEEE Microwave Wireless Compon Lett*. 2019;29(1):32-34.
12. Lee S, Lee Y. A planar dual-band filter based on reduced-length parallel coupled lines. *IEEE Microwave Wireless Compon Lett*. 2010;20(1):16-18.
13. Xu KD, Zhang FY, Liu YH, Liu QH. Bandpass filter using three pairs of coupled lines with multiple transmission zeros. *IEEE Microwave Wireless Compon Lett*. 2018;28(7):576-578.
14. Zhu H, Abbosh AM. Single- and dual-band bandpass filters using coupled stepped-impedance resonators with embedded coupled-lines. *IEEE Microwave Wireless Compon Lett*. 2016;26(9):675-677.
15. Li D, Xu K-D, Zhang A. Single-ended and balanced bandpass filters using multiple pairs of coupled lines and stepped-impedance stubs. *IEEE Access*. 2020;8:13541–13548.

How to cite this article: Xu J, Xu K-D, Zhang M, Chen Q. Dual-band bandpass filter using two simple coupled microstrip rings. *Engineering Reports*. 2021;3:e12288. https://doi.org/10.1002/eng2.12288